Biomacromolecules

pubs.acs.org/Biomac

Article

In Situ Synthesis and Self-Assembly of Peptide–PEG Conjugates: A Facile Method for the Construction of Fibrous Hydrogels

Published as part of Biomacromolecules virtual special issue "Peptide Materials".

Haritha Asokan-Sheeja, Kamal Awad, Jiazhu Xu, Myan Le, Jenny N. Nguyen, Na Nguyen, Tam P. Nguyen, Kytai T. Nguyen, Yi Hong, Venu G. Varanasi, Xiaohua Liu,* and He Dong*

Cite This: *Biomacromolecules* 2024, 25, 2814–2822

Read Online

ACCESS | Metrics & More | Article Recommendations | Supporting Information

ABSTRACT: Peptide-based hydrogels have gained considerable attention as a compelling platform for various biomedical applications in recent years. Their attractiveness stems from their ability to seamlessly integrate diverse properties, such as biocompatibility, biodegradability, easily adjustable hydrophilicity/hydrophobicity, and other functionalities. However, a significant drawback is that most of the functional self-assembling peptides cannot form robust hydrogels suitable for biological applications. In this study, we present the synthesis of novel peptide–PEG conjugates and explore their comprehensive hydrogel properties. The hydrogel comprises double networks, with the first network formed through the self-assembly of peptides to create a β-sheet secondary structure. The second network is established through covalent bond formation via *N*-hydroxysuccinimide chemistry between peptides and a 4-arm PEG to form a covalently linked network. Importantly, our findings reveal that this hydrogel formation method can be applied to other peptides containing lysine-rich sequences. Upon encapsulation of the hydrogel with antimicrobial peptides, the hydrogel retained high bacterial killing efficiency while showing minimum cytotoxicity toward mammalian cells. We hope that this method opens new avenues for the development of a novel class of peptide–polymer hydrogel materials with enhanced performance in biomedical contexts, particularly in reducing the potential for infection in applications of tissue regeneration and drug delivery.

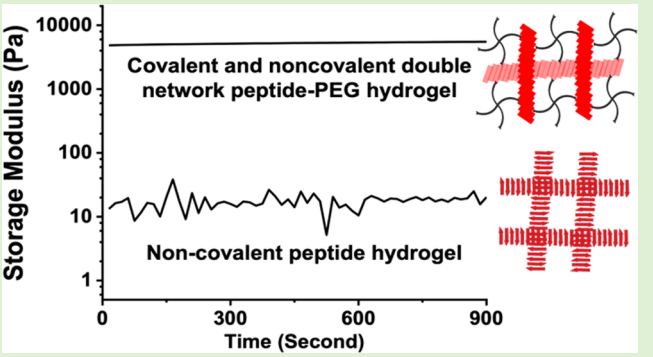

INTRODUCTION

Hydrogels represent a distinctive category of soft materials capable of retaining substantial amounts of water while preserving their intricate three-dimensional (3D) structures.[1−5] Among different types of hydrogel materials, peptide-based hydrogels show great biocompatibility, biodegradability, injectability, and tunable mechanical stability.[1,5−17] Over the past few decades, significant strides have been made in harnessing the potential of peptide hydrogels for therapeutic purposes, spanning diverse applications such as drug delivery, tissue engineering, wound healing, and biofabrication.[18−24] Peptide hydrogels are typically constructed through a self-assembly process that involves intricate supramolecular interactions unfolding along a hierarchical path in a concentration-dependent manner. At the pinnacle of this hierarchy lies the formation of hydrogels, which can be achieved through either chemical or physical cross-linking. Chemical cross-linking involves covalent bond formation, while noncovalent cross-linking relies on interactions such as hydrogen bonding, hydrophobic forces, electrostatic attractions, or van der Waals forces. In the past, most peptide-based hydrogels were characterized by a noncovalent network in which individual peptide fibrils are physically cross-linked with one another at a relatively high concentration. While the supramolecular network is effective in promoting hydrogel formation, the storage moduli of these soft hydrogels are relatively low. A few studies reported peptide assemblies with high storage moduli, but most of these systems require significant acidity, therefore having limited utility for biomedical applications.[25]

Compared to noncovalent peptide hydrogels, hydrogels based on covalent linking of multivalent polymers, such as polyethylene glycol (PEG), have improved rheological properties.[26−28] These gels have been widely explored in drug delivery and tissue engineering applications. Peptide–PEG

Received: December 27, 2023
Revised: March 28, 2024
Accepted: March 29, 2024
Published: April 10, 2024

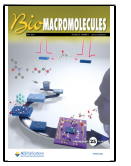

conjugates have also been used for the development of PEG hydrogels. Notably, the Yu group synthesized a collagen mimetic peptide (CMP)−PEG conjugate. The CMPs generated triple helix-mediated physical cross-links that increased the stiffness of the CMP−PEG hydrogel.[29] Inspired by these seminar work on PEG and PEG−peptide hydrogels, herein, we report a novel approach to synthesizing peptide hydrogels through a double network formation, employing a covalent *N*-hydroxysuccinimide (NHS) coupling reaction to generate peptide−PEG conjugates. The hydrogel consists of two essential components: (1) a lysine-rich self-assembling peptide characterized by an alternating hydrophobic−hydrophilic sequence, resulting in a sandwich-like β-sheet structure. The self-assembly of the peptide forms the first network within the hydrogel and (2) an NHS-activated PEG polymer, where the NHS group reacts with the amine side chains of the peptide, establishing the second network in the peptide hydrogel. The resulting double network significantly enhances the storage modulus of the peptide-based hydrogels. Furthermore, the method can be applicable to self-assembled peptides that cannot form hydrogels when they are standing alone. As shown in our study, for a viscous solution of self-assembled peptides, the introduction of the covalent network increases the storage moduli from 20 to 5500 Pa, therefore greatly expanding the utility of this approach. We expect that this innovative synthesis method will open new avenues for the construction of peptide-based hydrogels with tailored rheological properties and diverse biological functionalities for a range of biomedical applications.

EXPERIMENTAL SECTION

Materials. Fmoc-protected amino acids, hexafluorophosphate benzotriazole tetramethyluronium (HBTU), MBHA rink amide resin, piperidine, diisopropylethylamine (DIPEA), pyridine, Mueller Hinton Broth (MHB), and Agar were purchased from Sigma-Aldrich. Reagents and solvents for peptide synthesis and purification including dimethylformamide (DMF), acetonitrile (ACN), trifluoroacetic acid (TFA), triisopropylsilane (TIS), phosphate-buffered saline (PBS) 10×, and a live/dead bacterial viability kit were purchased from Fisher Scientific. 4-Arm PEG-GAS (M_W 20 k) was purchased from Creative PEG Works. Transmission electron microscopy (TEM) grids and uranium acetate dihydrate were purchased from Ted Pella, Inc. *Escherichia coli* (ATCC 25922) and Primary Dermal Fibroblast; Normal, Human, Adult (HDFa PCS-201−012) were purchased from ATCC.

Synthesis and Purification of Peptides. Fmoc solid-phase peptide synthesis procedures were used to synthesize the peptides on a Prelude peptide synthesizer at a 50 μmol scale using MBHA rink amide resin as the support. Fmoc groups were deprotected by 20% (v/v) piperidine in DMF for 5 min (2 times). Fmoc-protected amino acids, HBTU, and DIPEA (1:1:2) were dissolved in DMF and added to the resin reservoir. Upon completion of the synthesis, acetylation of the N-termini was performed in the presence of acetic anhydride and DIPEA in DMF. The peptides were cleaved from the resin using a mixture of TFA/TIS/H_2O (95/2.5/2.5 by volume) for 3 h. Through filtration, the cleavage solution was collected, and the resin was washed twice with neat TFA. Residual TFA was removed under moderate airflow. The residual peptide solution was precipitated with cold diethyl ether and then centrifuged 4 times. The crude peptide was dried under a vacuum overnight before HPLC purification. The peptide was purified using a preparative reverse-phase C4 column with a linear gradient of water/acetonitrile containing 0.05% TFA. Elution was monitored at 230 and 280 nm. The molecular mass was confirmed by MALDI-TOF MS. For P1, the calculated mass of $[M + Na]^+$ is 1376.60 and the experimental mass is 1376.46. For P2, the calculated mass of $[M + H]^+$ is 1296.63 and the experimental mass is 1296.85. For P3, the calculated mass of $[M + H]^+$ is 2147.68 and the experimental mass of $[M + H]^+$ is 2147.50. For P4, the calculated mass of $[M + H]^+$ is 3762.65 and the experimental mass is 3762.91.

Hydrogel Preparation. All hydrogels were prepared by reacting succinimidyl NHS-terminated PEGs with lysine-containing peptides at neutral pH. For example, to prepare 100 μL of gels, 2 mg of peptide and 1 mg of PEG were dissolved in 50 μL of DI water and mixed with an equal volume of PBS 2× to produce hydrogels at room temperature. Gel formation was examined by a vial inversion method.

Oscillatory Rheology. The rheological properties of hydrogels were characterized by oscillatory rheology using the Anton par MCR 702 Multidrive with a 10 mm stainless steel parallel plate geometry at 25 °C. A sample size of ∼200 μL of the hydrogel was delivered onto the rheometer plate, followed by an adjustment of the parallel plate geometry to have a gap height of 1 mm. A dynamic time sweep was performed first for 15 min (frequency: 6 rad/s, strain: 0.2%), followed by a dynamic frequency sweep (frequency range: 1−100 rad/s, strain: 0.2%). The hydrogel was then disrupted by a 1000% strain for 30 s at a frequency of 6 rad/s, followed by a dynamic time sweep (15 min, frequency: 6 rad/s, strain: 0.2%) to determine the storage modulus recovery. Finally, a dynamic strain sweep was performed on each hydrogel sample to determine the yield strain (strain range: 0.01−100%, frequency: 6 rad/s). For samples with very low storage modulus and loss modulus, only a dynamic time sweep was performed for 15 min (frequency: 6 rad/s, strain: 0.2%).

Live and Dead Assay for Bacterial Cells. A 400 μL aliquot of the bacterial suspension (*E. coli*, 10^9 CFU/mL) was seeded onto a glass-bottom dish and incubated at 37 °C for 24 h. The bacterial suspension was removed, and 1× PBS buffer was used to wash away any nonadherent bacteria. 50 μL of the hydrogel in 1× PBS and 100 μL of the Mueller Hinton Broth (MHB) medium were mixed and added to the dish. After incubation at 37 °C overnight, the MHB medium was removed and washed with PBS buffer 3 times. Bacteria were stained with the live/dead bacteria assay kit solution at room temperature for 30 min. Finally, the bacteria were washed with PBS buffer 3 times. Images were captured with an epifluorescence microscope and processed using ImageJ software.

Inhibition Zone Assay. 150 μL of the bacterial suspension (*E. coli*, 10^5 CFU/mL) was evenly streaked across an agar plate to ensure confluent growth and complete coverage of the surface. Subsequently, 100 μL of the hydrogel samples was carefully placed onto the surface of the agar plates. The plates were then incubated at 37 °C for 24 h. Following the incubation period, the agar plates were examined for the presence of inhibition zones surrounding the hydrogel samples, where no bacterial growth was observed. The diameter of these inhibition zones was measured and compared across the different samples to evaluate their antimicrobial efficacy.

Live and Dead Staining Assay for Mammalian Cells. The viability of HDFa cells on hydrogels was assessed using a live & dead viability/cytotoxicity kit (Invitrogen), wherein live cells are stained green with calcein AM and dead cells are stained red with ethidium homodimer-1 (EthD-1). After removal of the culture medium, samples were rinsed with PBS twice and treated with 2 μM calcein AM and 4 μM EthD-1 in DMEM for 30 min at 37 °C in the dark, followed by rinsing with PBS twice. Samples were directly observed under an inverted fluorescent microscope (Eclipse TiS, Nikon). Five randomly selected fields of view were imaged using an inverted fluorescent microscope. The obtained images were analyzed by ImageJ software, and the number of live and dead cells in each image was calculated. Cell viability is calculated by the following equation.

$$\text{cell viability} = \frac{\text{number of viable cells}}{\text{number of total cells}} \times 100\%$$

Hemolysis Assay. The peptide hydrogel hemocompatibility was tested using washed human red blood cells (hRBC) in 96-well plates following a previous protocol. Briefly, hRBCs were collected and washed from whole blood using centrifugation at 250*g* for 15 min. Then, the 96-well plate was coated with a 2% peptide hydrogel, and a 0.5% (v/v) diluted suspension of hRBC in PBS (1×) was added. PBS (1×) and 1% Triton X were used as the negative and positive

https://doi.org/10.1021/acs.biomac.3c01450
Biomacromolecules 2024, 25, 2814−2822

controls, respectively. The 96-well plates were incubated for 1 h at 37 °C on a shaker, and afterward, the plate was centrifuged at 1000*g* for 10 min. The hemolytic activity was analyzed through the supernatant's absorbance at 405 nm via spectrophotometry. Each assay was performed in quadruplicate. The percentage of hemolysis was calculated using the following equation.

$$\%\ \text{hemolysis} = \frac{(\text{absorbance of peptide} - \text{absorbance of PBS})}{(\text{absorbance of triton} - \text{absorbance of PBS})} \times 100\%$$

RESULTS AND DISCUSSION

Design and Synthesis of MDPs. All peptides were synthesized using a standard Fmoc solid-phase peptide synthesis strategy. Successful syntheses were confirmed via MALDI-TOF mass spectrometry (Figure S1A–D). Purification was assessed via high-performance liquid chromatography (HPLC), the chromatograms of which show a single product peak (Figure S1A–D). The primary sequences of the peptides used in this study are listed in Table 1.

Table 1. Peptide Sequences Used in This Study

name	N-	sequences	C-
P1	CH_3CO	K(QW)(QL)(QL)(QL)K	$CONH_2$
P2	CH_3CO	KK(QL)(QL)(QL)KK	$CONH_2$
P3	CH_3CO	KKK(QL)(QL)(QL)(QL)(QL)(QL)KK	$CONH_2$
P4	CH_3CO	KKKKKKKK(QF)(QF)(QF)(QF)(QF)(QF)KKKKKKKK	$CONH_2$

All of the peptides are N-terminally acetylated and C-terminally amidated. The self-assembling peptide sequence, denoted P1, was formulated based on our prior investigation of the MDP sequence $K_X(QL)_YK_Z$ (with K representing lysine, Q representing glutamine, and L representing leucine). In this context, *X*, *Y*, and *Z* represent the number of repeating units. To simplify synthesis and enable scalability, we designed the sequence $K(QW)(QL)_3K$, where $X = 1$, $Y = 4$, and $Z = 1$ with one of the L residues replaced by W (tryptophan) for ultraviolet–visible (UV–vis)-based concentration measurements. As demonstrated in our previous research,[30−34] the alternating hydrophilic–hydrophobic pattern of (QW)(QL)3 promotes the formation of sandwich-like nanofiber structures with leucines and tryptophan embedded within the hydrophobic core of the assembly. The specific values chosen for *X*, *Y*, and *Z* were intended to enhance the solubility of the peptide assemblies while preserving the formation of secondary structures, as established in prior work.[14,35−37]

Molecular Design, Synthesis, and Characterization of Peptide–PEG Hydrogels. The peptide–PEG hybrid hydrogel was synthesized via an NHS–amine reaction between lysine-containing self-assembling peptide P1 and a 4-arm PEG terminated with an NHS ester. P1 was first dissolved in deionized water at a concentration of 4 wt % and further mixed with an equal volume of PBS buffer (2×). The overall ionic strength of the solution and especially the presence of oppositely charged multivalent ions such as phosphate result in quenching the repulsive charges between peptides and the growth of nanofibers to form a weak hydrogel. When PEG is introduced, it significantly enhances the hydrogel's strength through covalent bond formation between the amine groups in the peptide and the reactive NHS group in the PEG. This results in the formation of a double-network P1–PEG hydrogel. The first network consists of self-assembled P1 nanofibers, while the second network is established by covalently cross-linking between P1 and PEG, as illustrated in Scheme 1.

To assess the strength of the formed hydrogel, we employed a vial inversion test. In contrast to P1, which yields a highly viscous solution (Figure 1a), P1–PEG generates a remarkably robust hydrogel (Figure 1b).

P1 or P1–PEG was dissolved in a PBS solution for the examination of secondary structure formation and macroscopic assembly using circular dichroism (CD) spectroscopy. The CD measurement solution was prepared by diluting the peptide stock solution, initially at 2 wt % in water, with PBS to achieve a final concentration of 0.02 wt %. As anticipated based on the MDP design, CD analysis of P1 revealed a distinct β-sheet structure with a maximum at 198 nm and a minimum at 218 nm (Figure 2a). Following the addition of PEG to P1 to generate PEG–P1, the secondary structure remained largely unchanged, exhibiting a predominant β-sheet structure on CD. Transmission electron microscopy (TEM) further substantiated the self-assembly, illustrating the formation of long nanofibers for P1, whereas PEG–P1 exhibited shorter nanofibers (Figure 2b,c).

To identify the effect of the PEG/peptide ratio on the hydrogel strength, a dynamic oscillatory time sweep was conducted. Hydrogels were prepared by systematically adjust-

Scheme 1. Schematic Representation of Peptide–PEG Hydrogel Formation[a]

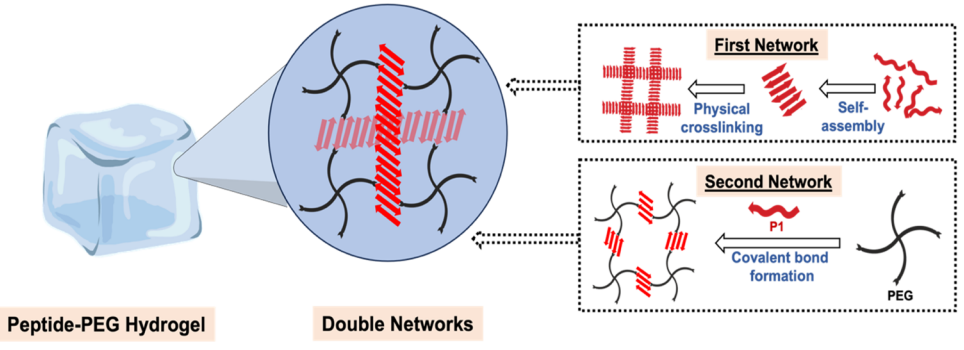

[a]The first network is formed by the self-assembly of the peptide into sandwich-like supramolecular nanofibers that are physically cross-linked with each other, and the second network is formed by the covalent formation between the NHS moiety in the PEG and amine residues in the peptide to form a double-network hydrogel.

https://doi.org/10.1021/acs.biomac.3c01450
Biomacromolecules 2024, 25, 2814–2822

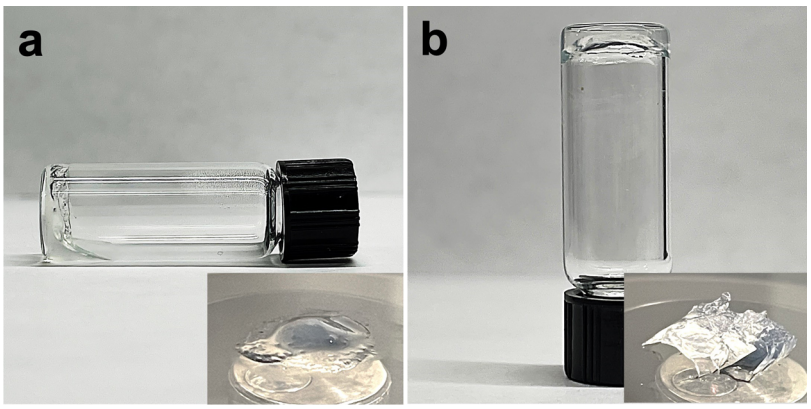

Figure 1. Vial inversion method for assessing hydrogel strength. (a) P1 (2 wt %) in PBS 1× forms a weak hydrogel due to the self-assembly of P1. (b) Addition of PEG (1 wt %) to P1, forming P1−PEG in PBS 1×, results in the formation of a highly rigid hydrogel due to the covalent bonds connecting the self-assembly. Incubation time: 2 h.

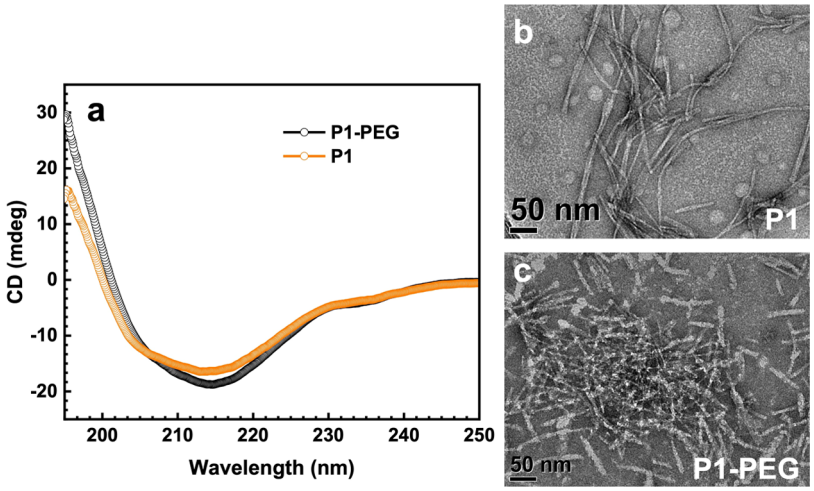

Figure 2. (a) CD spectra of peptide hydrogel P1 and P1−PEG showing the β-sheet conformation as characterized by the negative absorption at 215 nm. TEM images of (b) P1 and (c) P1−PEG.

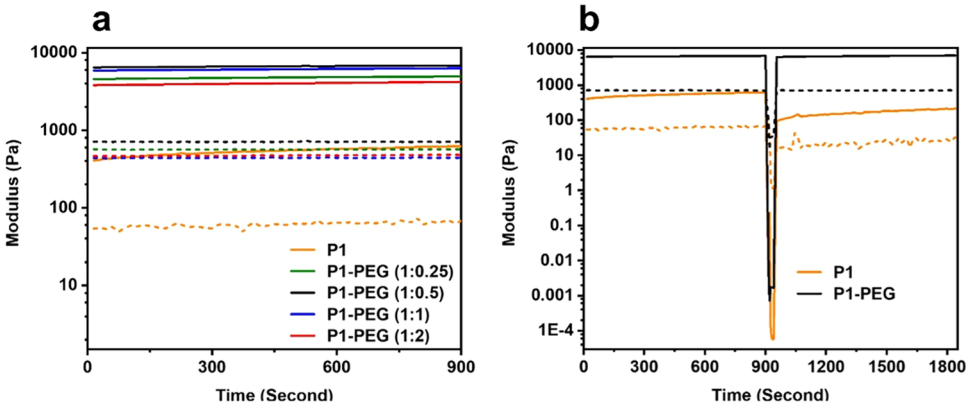

Figure 3. (a) Rheological properties of the peptide hydrogel (2 wt %) containing different ratios of PEG during time sweep (frequency: 6 rad/s, strain: 0.2%). (b) Dynamic time sweep of P1 and the strongest P1−PEG gel (1:0.5) over 900 s (frequency: 6 rad/s, strain: 0.2%). At the 900th s, a 1000% strain was applied to completely disrupt the hydrogel, and the subsequent recovery of storage modulus was continuously measured. Solid line: storage modulus; dashed line: loss modulus.

ing the PEG ratio while keeping the peptide concentration constant at 2 wt %. In all peptide hydrogels, the storage modulus (G') significantly exceeded the loss modulus (G'') within the relevant linear viscoelastic region, confirming the formation of an elastic hydrogel (Figure 3a). Oscillatory time sweep experiments, conducted under an angular frequency of 6 rad/s and 0.2% strain for 900 s, revealed that the peptide alone formed a hydrogel with a storage modulus of ∼620 Pa and a loss modulus of ∼62 Pa. Upon adding PEG with a P1−PEG weight ratio of 1:0.25, both the storage and loss moduli

https://doi.org/10.1021/acs.biomac.3c01450
Biomacromolecules 2024, 25, 2814−2822

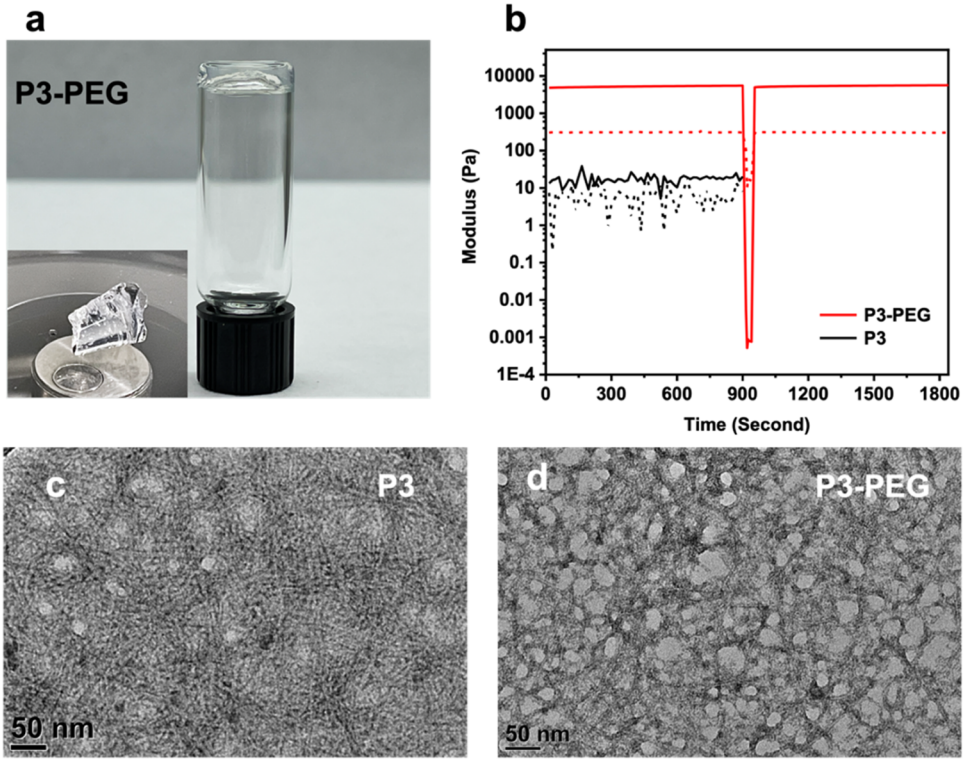

Figure 4. (a) Photograph showing the formation of the P3−PEG hydrogel. (b) Rheological properties of P3 and P3−PEG hydrogels during a time sweep (frequency: 6 rad/s, strain: 0.2%). At the 900th s, P3−PEG was completely disrupted using 1000% strain, and the subsequent recovery of storage modulus was continuously measured. The solid line represents the storage modulus, while the dashed line represents the loss modulus. TEM images of (c) P3 and (d) P3−PEG reveal the presence of long nanofibers.

increased significantly, attributed to the augmented covalent bonds connecting nanofibers formed by P1 self-assembly. Increasing the weight ratio to 1:0.5 further enhanced the hydrogel strength, demonstrating the positive effect of increased PEG content on covalent connectivity between nanofibers. However, beyond a 1:1 ratio, rigidity slightly decreased, possibly due to saturation of reactive amine ends or reduced quality of self-assembly with higher polymer content. The 1:2 ratio resulted in a further decline in hydrogel strength (Figure S2). The strongest hydrogel was formed by P1−PEG (1:0.5), exhibiting a substantial storage modulus of ∼6800 Pa and loss modulus of ∼710 Pa. Dynamic oscillatory frequency sweep analysis across different P1−PEG ratios demonstrated that the 1:0.5 ratio exhibited weak frequency dependence from 0.1 to 100 rad/s, outperforming other P1−PEG gels (Figure S3). Dynamic strain sweep experiments confirmed the mechanical stability, with P1−PEG (1:0.5) displaying the highest yield point at 16% compared with other P1−PEG gels and pure P1 (Figure S4). Based on rheology measurements, the P1−PEG (1:0.5) ratio was determined to form the optimal hydrogel, and this ratio was utilized in all subsequent experiments. To assess the injectability of P1−PEG, a dynamic time sweep was performed (Figure 3b). Measurements at an angular frequency of 6 rad/s and 0.2% strain for 15 min, followed by an increase to 1000% strain to disrupt the hydrogel, showed ∼100% recovery for P1−PEG, indicating its potential as an injectable hydrogel for biological applications. It is worth noting that this rapid shear thinning and recovery persisted after four cycles (Figure S5). In contrast, P1 gels did not exhibit robust recovery after disruption, emphasizing the advantages of using P1−PEG hydrogels in biological applications.

The significance of self-assembly was assessed using a monomeric peptide, P2. The CD spectra of P2 exhibited a characteristic minimum at 195 nm, confirming a random coil secondary structure of P2 (Figure S5). This outcome aligns with expectations, considering that for long-range assemblies, the packing of only three leucine residues must compensate for the charge repulsion of four lysine residues. The vial inversion method revealed that P2−PEG formed a viscous liquid (Figure S7), indicating that without the first network or the self-assembly of the peptide, the second network alone could not create a rigid hydrogel structure. Consequently, self-assembly plays a crucial role in augmenting the rigidity of the hydrogel. To validate this observation, a dynamic time sweep was conducted for 15 min under an angular frequency of 6 rad/s and 0.2% strain to measure the storage modulus and loss modulus of the PEG−P2 sample, assessing hydrogel strength (Figure S8). P2−PEG exhibited a liquid-like consistency with a storage modulus of ∼16 Pa and a loss modulus of ∼4 Pa. These results affirm our hypothesis that the self-assembling nature of the peptide is essential for the formation of a rigid hydrogel.

To assess the significance of the second network, involving covalent bond formation between P1 and PEG, we substituted NHS ester-terminated PEG with carboxylic acid-terminated PEG_{COOH} to create PEG_{COOH}−P1. Due to the absence of a reactive NHS group, there is no covalent bonding between P1 and PEG_{COOH}. The vial inversion method revealed that PEG_{COOH}−P1 forms a weaker gel compared to P1 gel (Figure S9). Oscillatory time sweep measurements of PEG_{COOH}−P1

https://doi.org/10.1021/acs.biomac.3c01450
Biomacromolecules 2024, 25, 2814−2822

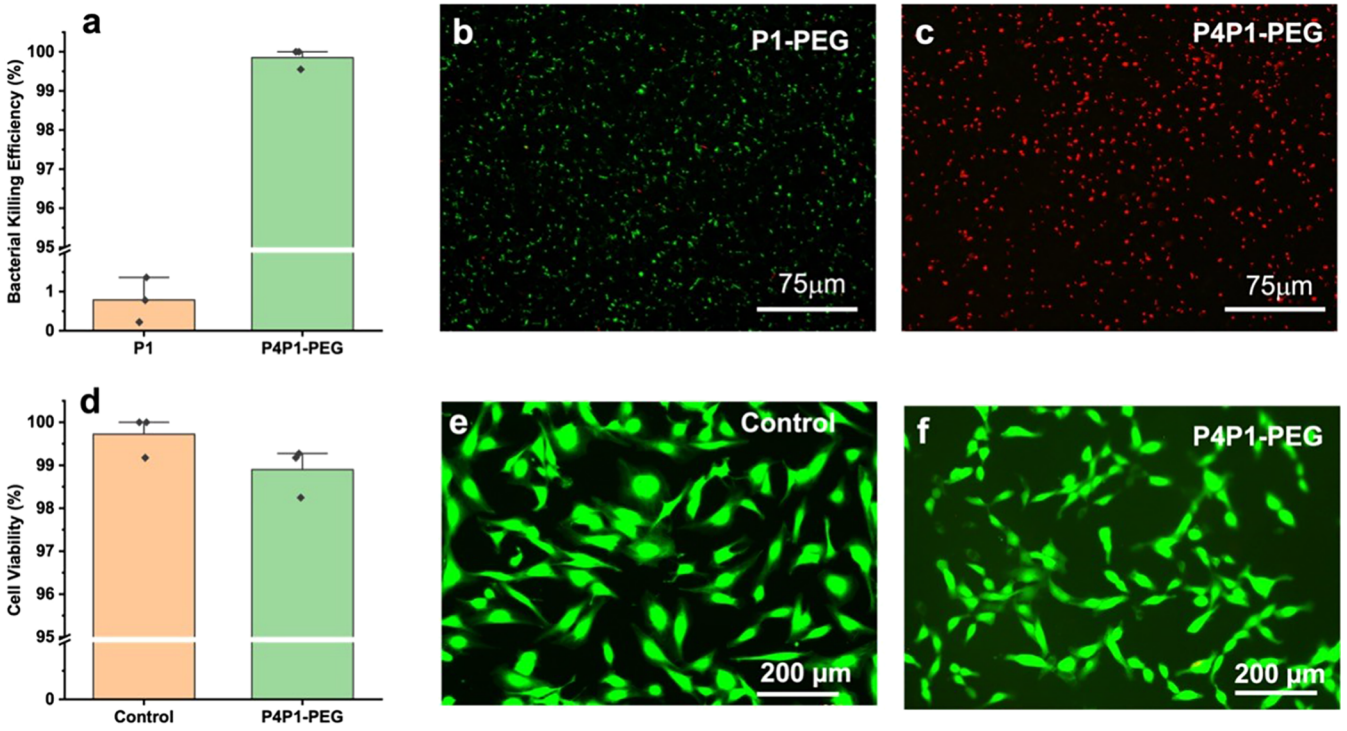

Figure 5. Top panel: (a) Bacterial killing efficiency assay of P1−PEG and P4P1−PEG hydrogels against *E. coli* after 24 h. Fluorescence microscopy images of *E. coli* through live and dead assays for (b) P1−PEG and (c) P4P1−PEG. Live bacteria were stained with SYTO9 (green), and dead bacteria were stained with PI (red). Bottom panel: (d) Cell viability of HDFa cells in the presence and absence (control) of P4P1−PEG gels after 24 h. Fluorescence microscopic images of HDFa cells through live and dead assays for (e) control and (f) cells incubated with P4P1−PEG after 24 h. Live cells are stained green with calcein AM, and dead cells are stained red with ethidium homodimer-1.

indicated that the resulting weaker gel had storage modulus and loss modulus values of 87 and 17 Pa, respectively (Figure S10). The time sweep demonstrated that over a 15-min period under an angular frequency of 6 rad/s and 0.2% strain, PEG_{COOH}−P1 behaved as a weak gel. These observations underscore the importance of the second network, specifically covalent bond formation, in enhancing hydrogel strength. Combining these results, both self-assembly and covalent bonding are crucial for effective hydrogel formation.

We proceeded to investigate if this method can be used for other amine-rich self-assembling peptides. Another self-assembling peptide, P3, was used as a model to test if this method can be generalized. P3 contains five lysine residues that can be used for making bonds with the NHS group. P3 at 2 wt % concentration forms a viscous solution, and no hydrogel formation was observed in PBS. After the addition of 1 wt % PEG, a strong hydrogel was formed. The hydrogel formation was confirmed by the vial inversion method (Figure 4a). TEM was used to confirm the formation of self-assembly in P3, showing an extensive network of nanofibers (Figure 4c), which was also observed in P3−PEG (Figure 4d), indicating the formation of the first network, which is the self-assembly. The rheology measurements were used to characterize hydrogel formation. Dynamic time sweep measurements unveiled a significant elevation in both storage modulus (5500 Pa) and loss modulus (300 Pa) for P3−PEG compared to P3 alone (20 and 6 Pa, respectively), as shown in Figure 4b. The markedly higher storage modulus indicated the formation of an elastic hydrogel. To evaluate the self-recovery of P3−PEG, a high (1000%) strain was applied for 15 min to completely disrupt the gel. Subsequently, rapid recovery at low strain was observed, mirroring the trend observed in P1−PEG gels. Dynamic frequency sweep measurements indicated minimal frequency dependence in these gels (Figure S11). A strain sweep from 0.01 to 100% on P3−PEG revealed shear-yielding behavior at high strain, with a crossover of storage/loss modulus occurring around 16%, aligning with the behavior observed in P1−PEG gels (Figure S12).

Evaluation of the Antimicrobial Activity and Cytotoxicity of Peptide−PEG Hydrogels. Synthetic antimicrobial peptides (AMP) can be easily integrated into hydrogels. Specifically, we used a cationic AMP featuring the sequence $K_8(QF)_6K_8$, where the subscript denotes the repeating units of K (lysine) and the binary QF motif (Q: glutamine, F: phenylalanine). P4 was designed to have the amphiphilic structure of a conical AMP. The MIC of P4 was determined to be 2.5 μM against *E. coli*. Due to the alternating hydrophobic and hydrophilic residue pattern, P4 is expected to have a favorable interaction with P1, which has the same pattern. Therefore, it can be immobilized within or on the surface of the hydrogel network and provide the desired antimicrobial activity to hydrogels. Initial antibacterial assessments of the P1−PEG hydrogel revealed a lack of significant antibacterial properties. To enhance the antibacterial efficacy, P4 (5% of the total weight) was introduced to the hydrogel, resulting in the formation of hydrogels denoted P4P1 (Figure S13). TEM images of P4P1−PEG show the formation of nanofibers, confirming the self-assembly in the presence of P4 (Figure S14). The incorporation of P4 led to a reduction in hydrogel strength compared to P1−PEG alone (3750 vs 6800 Pa), likely due to partial disruption of the fibrous packing between P1 (Figure S15). Nevertheless, the storage modulus is still higher than typical peptide-based hydrogels, and our hydrogels are suitable for various biological applications. Moreover, the time

https://doi.org/10.1021/acs.biomac.3c01450
Biomacromolecules 2024, 25, 2814−2822

sweep data underscored P4P1−PEG's excellent recovery capability under 1000% strain, highlighting its potential for efficient injectability. Dynamic frequency sweep analysis revealed negligible frequency dependency within the P4P1−PEG hydrogels, as depicted in Figure S16, signifying the stability of their mechanical properties across different frequencies. Furthermore, a strain sweep spanning from 0.01 to 100% elucidated shear-yielding behavior at elevated strains, with a crossover of storage/loss modulus observed at 17%, mirroring the behavior observed in P1−PEG gels (Figure S17). Antibacterial assays conducted against *E. coli* demonstrated a remarkable bacterial killing efficiency (nearly 100%) for the P4P1−PEG hydrogels (Figure 5a). To ascertain whether the enhanced antibacterial effect was solely attributed to the antibacterial hydrogel or if it resulted from the released P4 peptide, a control experiment was conducted. The P4P1−PEG hydrogel was incubated in PBS buffer for 24 h, after which all supernatant was removed before the bacterial killing assay. This control group is denoted P4P1−PEG*. Interestingly, P4P1−PEG* demonstrated impressive antibacterial efficacy, albeit slightly lower compared to P4P1−PEG gels, suggesting that the antibacterial effect of hydrogels is not solely due to the presence of loose peptides but is also attributed to the encapsulated P4 (Figure S18). The enhanced antimicrobial activity of P4P1−PEG was further confirmed through a bacterial live and dead assay of *E. coli* treated with P1−PEG and P4P1−PEG gels, as shown in Figure 5b,c. Larger number of dead bacteria was observed for *E. coli* treated with P4P1−PEG, whereas P1−PEG showed no significant bacterial killing. To further assess the antimicrobial characteristics of the hydrogel, an inhibition zone assay was conducted (Figure S19). P4P1−PEG gels exhibited an inhibition zone extending 30 mm around the gel, whereas no distinct inhibition zone was noted around the P1−PEG gel, consistent with the bacterial live and dead assay results.

We evaluated the cytotoxicity of P4P1−PEG toward HDFa cells by incubating cells with P4P1−PEG. The results show that P4P1−PEG exhibited good cytocompatibility (Figure 5d) with ∼99% cell viability. Live and dead assays show that most of the cells are viable after 24 h of incubation with the gels (Figure 5e,f). Furthermore, the hemolysis assessment was conducted to evaluate the hemocompatibility by exposing hRBCs to the gel at 37 °C for 1 h. The hemolytic rate was quantified by measuring the amount of hemoglobin released in the supernatant via absorbance at 405 nm using a spectrophotometer. Compared with the positive control (Triton X), P4P1−PEG and P1−PEG only showed minor hemolysis, with values of 1.17, and 1.05%, respectively, as shown in Figure S20, indicating that the gel was exceptionally hemocompatible. The high antimicrobial activity and low cytotoxicity of P4P1−PEG make these gels useful for the treatment of bacterial infections.

CONCLUSIONS

We demonstrated an efficient method for synthesizing double-network peptide−polymer hydrogels. The incorporation of lysine-containing self-assembling peptides with NHS-group-containing PEG results in the formation of covalent bonds, thereby reinforcing the interactions between the self-assembled peptides. This covalent linkage strengthens the overall structure of the hydrogel. Notably, the formed hydrogel exhibits robust recovery after complete disruption, highlighting excellent injectability. Furthermore, our study reveals the versatility of this hydrogel formation method, extending its application to other self-assembling peptides with reactive amine groups. The conversion of self-assembling peptides into injectable hydrogels holds immense potential for biomedical applications, particularly in targeted delivery systems. As part of an application study, we encapsulated the hydrogel with antimicrobial peptides (AMPs), resulting in an antimicrobial hydrogel. The outcomes demonstrate that the antimicrobial hydrogel exhibits approximately 100% bacterial killing efficacy with minimal cytotoxicity. This underscores the promising prospects of our method in the development of advanced biomedical solutions, particularly in the realm of targeted antimicrobial delivery.

ASSOCIATED CONTENT

Supporting Information

The Supporting Information is available free of charge at https://pubs.acs.org/doi/10.1021/acs.biomac.3c01450.

Characterization of the chemical compositions and physical properties and antibacterial properties of PEG−peptide conjugates (PDF)

AUTHOR INFORMATION

Corresponding Authors

Xiaohua Liu − *Department of Chemical and Biomedical Engineering, The University of Missouri, Columbia, Missouri 65211, United States;* orcid.org/0000-0003-0177-0886; Email: xlz2y@missouri.edu

He Dong − *Department of Chemistry & Biochemistry, The University of Texas at Arlington, Arlington, Texas 76019, United States;* orcid.org/0000-0002-8494-0475; Email: he.dong@uta.edu

Authors

Haritha Asokan-Sheeja − *Department of Chemistry & Biochemistry, The University of Texas at Arlington, Arlington, Texas 76019, United States*

Kamal Awad − *Bone Muscle Research Center, The University of Texas at Arlington, Arlington, Texas 76019, United States*

Jiazhu Xu − *Department of Bioengineering, The University of Texas at Arlington, Arlington, Texas 76019, United States*

Myan Le − *Department of Chemistry & Biochemistry, The University of Texas at Arlington, Arlington, Texas 76019, United States*

Jenny N. Nguyen − *Department of Chemistry & Biochemistry, The University of Texas at Arlington, Arlington, Texas 76019, United States*

Na Nguyen − *Department of Bioengineering, The University of Texas at Arlington, Arlington, Texas 76019, United States*

Tam P. Nguyen − *Department of Bioengineering, The University of Texas at Arlington, Arlington, Texas 76019, United States*

Kytai T. Nguyen − *Department of Bioengineering, The University of Texas at Arlington, Arlington, Texas 76019, United States*

Yi Hong − *Department of Bioengineering, The University of Texas at Arlington, Arlington, Texas 76019, United States;* orcid.org/0000-0002-5846-2596

Venu G. Varanasi − *Bone Muscle Research Center, The University of Texas at Arlington, Arlington, Texas 76019, United States*

Complete contact information is available at:

https://doi.org/10.1021/acs.biomac.3c01450
Biomacromolecules 2024, 25, 2814−2822

https://pubs.acs.org/10.1021/acs.biomac.3c01450

Author Contributions

All authors have given approval to the final version of the manuscript.

Notes

The authors declare no competing financial interest.

■ ACKNOWLEDGMENTS

This study was supported by the National Science Foundation (DMR 1824614 and DMR 1341925) and the start-up funds from the University of Texas at Arlington. The authors would also like to thank the National Institutes of Health/National Institute of Dental and Craniofacial Research (NIH/NIDCR grant number R01 DE031872, Varanasi, PI) for their support.

■ REFERENCES

(1) Jonker, A. M.; Löwik, D. W. P. M.; van Hest, J. C. M. Peptide- and Protein-Based Hydrogels. *Chem. Mater.* **2012**, *24* (5), 759−773.
(2) Lee, K. Y.; Mooney, D. J. Hydrogels for Tissue Engineering. *Chem. Rev.* **2001**, *101* (7), 1869−1880.
(3) Mondal, S.; Das, S.; Nandi, A. K. A review on recent advances in polymer and peptide hydrogels. *Soft Matter* **2020**, *16* (6), 1404−1454.
(4) Van Vlierberghe, S.; Dubruel, P.; Schacht, E. Biopolymer-Based Hydrogels As Scaffolds for Tissue Engineering Applications: A Review. *Biomacromolecules* **2011**, *12* (5), 1387−1408.
(5) Yan, C.; Pochan, D. J. Rheological properties of peptide-based hydrogels for biomedical and other applications. *Chem. Soc. Rev.* **2010**, *39* (9), 3528−3540.
(6) Aulisa, L.; Dong, H.; Hartgerink, J. D. Self-Assembly of Multidomain Peptides: Sequence Variation Allows Control over Cross-Linking and Viscoelasticity. *Biomacromolecules* **2009**, *10* (9), 2694−2698.
(7) Chen, W.; Hazoor, S.; Madigan, R.; Adones, A. A.; Chintapula, U. K.; Nguyen, K. T.; Tang, L.; Foss, F. W.; Dong, H. Alkaline-responsive polydiacetylene-peptide hydrogel for pH-sensing and on-demand antimicrobial release. *Mater. Today Adv.* **2022**, *16*, No. 100288.
(8) Jiang, L.; Xu, D.; Sellati, T. J.; Dong, H. Self-assembly of cationic multidomain peptide hydrogels: supramolecular nanostructure and rheological properties dictate antimicrobial activity. *Nanoscale* **2015**, *7* (45), 19160−19169.
(9) Li, J.; Xing, R.; Bai, S.; Yan, X. Recent advances of self-assembling peptide-based hydrogels for biomedical applications. *Soft Matter* **2019**, *15* (8), 1704−1715.
(10) Lin, B. F.; Megley, K. A.; Viswanathan, N.; Krogstad, D. V.; Drews, L. B.; Kade, M. J.; Qian, Y.; Tirrell, M. V. pH-responsive branched peptide amphiphile hydrogel designed for applications in regenerative medicine with potential as injectable tissue scaffolds. *J. Mater. Chem. B* **2012**, *22* (37), 19447−19454.
(11) Majumder, P.; Singh, A.; Wang, Z.; Dutta, K.; Pahwa, R.; Liang, C.; Andrews, C.; Patel, N. L.; Shi, J.; de Val, N.; et al. Surface-fill hydrogel attenuates the oncogenic signature of complex anatomical surface cancer in a single application. *Nat. Nanotechnol.* **2021**, *16* (11), 1251−1259.
(12) Weingarten, A. S.; Kazantsev, R. V.; Palmer, L. C.; McClendon, M.; Koltonow, A. R.; Samuel, A. P. S.; Kiebala, D. J.; Wasielewski, M. R.; Stupp, S. I. Self-assembling hydrogel scaffolds for photocatalytic hydrogen production. *Nat. Chem.* **2014**, *6* (11), 964−970.
(13) Xue, B.; Bashir, Z.; Guo, Y.; Yu, W.; Sun, W.; Li, Y.; Zhang, Y.; Qin, M.; Wang, W.; Cao, Y. Strong, tough, rapid-recovery, and fatigue-resistant hydrogels made of picot peptide fibres. *Nat. Chem.* **2023**, *14* (1), No. 2583, DOI: 10.1038/s41467-023-38280-4.
(14) Dong, H.; Paramonov, S. E.; Aulisa, L.; Bakota, E. L.; Hartgerink, J. D. Self-Assembly of Multidomain Peptides: Balancing Molecular Frustration Controls Conformation and Nanostructure. *J. Am. Chem. Soc.* **2007**, *129* (41), 12468−12472.
(15) Swanekamp, R. J.; Welch, J. J.; Nilsson, B. L. Proteolytic stability of amphipathic peptide hydrogels composed of self-assembled pleated β-sheet or coassembled rippled β-sheet fibrils. *Chem. Commun.* **2014**, *50* (70), 10133−10136.
(16) Du, X.; Zhou, J.; Shi, J.; Xu, B. Supramolecular Hydrogelators and Hydrogels: From Soft Matter to Molecular Biomaterials. *Chem. Rev.* **2015**, *115* (24), 13165−13307.
(17) Yang, Z.; Ho, P.-L.; Liang, G.; Chow, K. H.; Wang, Q.; Cao, Y.; Guo, Z.; Xu, B. Using β-Lactamase to Trigger Supramolecular Hydrogelation. *J. Am. Chem. Soc.* **2007**, *129* (2), 266−267.
(18) Falcone, N.; Ermis, M.; Tamay, D. G.; Mecwan, M.; Monirizad, M.; Mathes, T. G.; Jucaud, V.; Choroomi, A.; de Barros, N. R.; Zhu, Y.; et al. Peptide Hydrogels as Immunomaterials and Their Use in Cancer Immunotherapy Delivery. *Adv. Healthc. Mater.* **2023**, *12* (27), No. 2301096.
(19) Mukherjee, N.; Adak, A.; Ghosh, S. Recent trends in the development of peptide and protein-based hydrogel therapeutics for the healing of CNS injury. *Soft Matter* **2020**, *16* (44), 10046−10064.
(20) Nambiar, M.; Schneider, J. P. Peptide hydrogels for affinity-controlled release of therapeutic cargo: Current and potential strategies. *J. Pept. Sci.* **2022**, *28* (1), No. e3377.
(21) Roy, K.; Pandit, G.; Chetia, M.; Sarkar, A. K.; Chowdhuri, S.; Bidkar, A. P.; Chatterjee, S. Peptide Hydrogels as Platforms for Sustained Release of Antimicrobial and Antitumor Drugs and Proteins. *ACS Appl. Bio Mater.* **2020**, *3* (9), 6251−6262.
(22) Thota, C. K.; Yadav, N.; Chauhan, V. S. A novel highly stable and injectable hydrogel based on a conformationally restricted ultrashort peptide. *Sci. Rep.* **2016**, *6* (1), No. 31167.
(23) Wang, F.; Su, H.; Wang, Z.; Anderson, C. F.; Sun, X.; Wang, H.; Laffont, P.; Hanes, J.; Cui, H. Supramolecular Filament Hydrogel as a Universal Immunomodulator Carrier for Immunotherapy Combinations. *ACS Nano* **2023**, *17* (11), 10651−10664.
(24) Zhang, Z.; Ai, S.; Yang, Z.; Li, X. Peptide-based supramolecular hydrogels for local drug delivery. *Adv. Drug Delivery Rev.* **2021**, *174*, 482−503.
(25) Clarke, D. E.; Parmenter, C. D. J.; Scherman, O. A. Tunable Pentapeptide Self-Assembled β-Sheet Hydrogels. *Angew. Chem., Int. Ed.* **2018**, *57* (26), 7709−7713.
(26) DeForest, C. A.; Sims, E. A.; Anseth, K. S. Peptide-Functionalized Click Hydrogels with Independently Tunable Mechanics and Chemical Functionality for 3D Cell Culture. *Chem. Mater.* **2010**, *22* (16), 4783−4790.
(27) Kyburz, K. A.; Anseth, K. S. Three-dimensional hMSC motility within peptide-functionalized PEG-based hydrogels of varying adhesivity and crosslinking density. *Acta Biomater.* **2013**, *9* (5), 6381−6392.
(28) Lin, C.-C.; Metters, A. T.; Anseth, K. S. Functional PEG−peptide hydrogels to modulate local inflammation inducedby the pro-inflammatory cytokine TNFα. *Biomaterials* **2009**, *30* (28), 4907−4914.
(29) Stahl, P. J.; Romano, N. H.; Wirtz, D.; Yu, S. M. PEG-Based Hydrogels with Collagen Mimetic Peptide-Mediated and Tunable Physical Cross-Links. *Biomacromolecules* **2010**, *11* (9), 2336−2344.
(30) Asokan-Sheeja, H.; Yang, S.; Adones, A. A.; Chen, W.; Fulton, B. B.; Chintapula, U. K.; Nguyen, K. T.; Lovely, C. J.; Brautigam, C. A.; Nam, K.; Dong, H. Self-assembling Peptides with Internal Ionizable Unnatural Amino Acids: A General Approach to pH-responsive Peptide Materials. *Chem. - Asian J.* **2022**, *17* (19), No. e202200724.
(31) Chen, W.; Li, S.; Renick, P.; Yang, S.; Pandy, N.; Boutte, C.; Nguyen, K. T.; Tang, L.; Dong, H. Bacterial acidity-triggered antimicrobial activity of self-assembling peptide nanofibers. *J. Mater. Chem. B* **2019**, *7* (18), 2915−2919.
(32) Xu, D.; Chen, W.; Tobin-Miyaji, Y. J.; Sturge, C. R.; Yang, S.; Elmore, B.; Singh, A.; Pybus, C.; Greenberg, D. E.; Sellati, T. J.; et al. Fabrication and Microscopic and Spectroscopic Characterization of Cytocompatible Self-Assembling Antimicrobial Nanofibers. *ACS Infect. Dis.* **2018**, *4* (9), 1327−1335.

(33) Xu, D.; Jiang, L.; Singh, A.; Dustin, D.; Yang, M.; Liu, L.; Lund, R.; Sellati, T. J.; Dong, H. Designed supramolecular filamentous peptides: balance of nanostructure, cytotoxicity and antimicrobial activity. *Chem. Commun.* **2015**, *51* (7), 1289−1292.
(34) Xu, D.; Samways, D. S. K.; Dong, H. Fabrication of self-assembling nanofibers with optimal cell uptake and therapeutic delivery efficacy. *Bioact. Mater.* **2017**, *2* (4), 260−268.
(35) Xu, D.; Ran, Q.; Xiang, Y.; Jiang, L.; Smith, B. M.; Bou-Abdallah, F.; Lund, R.; Li, Z.; Dong, H. Toward hemocompatible self-assembling antimicrobial nanofibers: understanding the synergistic effect of supramolecular structure and PEGylation on hemocompatibility. *RSC Adv.* **2016**, *6* (19), 15911−15919.
(36) Yang, S.; Dong, H. Modular design and self-assembly of multidomain peptides towards cytocompatible supramolecular cell penetrating nanofibers. *RSC Adv.* **2020**, *10* (49), 29469−29474.
(37) Xu, D.; Dustin, D.; Jiang, L.; Samways, D. S. K.; Dong, H. Designed filamentous cell penetrating peptides: probing supramolecular structure-dependent membrane activity and transfection efficiency. *Chem. Commun.* **2015**, *51* (59), 11757−11760.

https://doi.org/10.1021/acs.biomac.3c01450
Biomacromolecules 2024, 25, 2814−2822